Journal of Environmental Chemical Engineering 11 (2023) 109801

Contents lists available at ScienceDirect

Journal of Environmental Chemical Engineering

journal homepage: www.elsevier.com/locate/jece

Implanting nitrogen-doped graphene quantum dots on porous ultrathin carbon nitride for efficient metal-free photocatalytic hydrogen evolution

Hanxiang Chen [a,b], Zhao Mo [a,*], Zeming Wang [c], Pengcheng Yan [a], Peipei Sun [a], Guanyu Wu [a], Jinyuan Zhang [a], Xianglin Zhu [a], Liang Wang [c,*], Hui Xu [a,*]

[a] School of the Environment and Safety Engineering, School of Materials Science & Engineering, Institute for Energy Research, Jiangsu University, Zhenjiang 212013, PR China

[b] Department of Applied Biology and Chemical Technology, The Hong Kong Polytechnic University, Hung Hom, Kowloon, Hong Kong Special Administrative Region of China

[c] Institute of Nanochemistry and Nanobiology, School of Environmental and Chemical Engineering, Shanghai University, Shanghai 200444, PR China

ARTICLE INFO

Editor: Pei Xu

Keywords:
Carbon nitride
Nitrogen-doped graphene quantum dots
Photocatalysis
Hydrogen evolution
Water splitting

ABSTRACT

Mimicking natural photosynthesis to make solar power into hydrogen energy is widely perceived as a promising and sustainable way to alleviate the energy crisis and environmental pollution. However, adding metallic co-catalysts and even noble metal cocatalysts into carbon nitride-based photocatalysts still seriously restrict the practical development of photocatalytic water splitting. To address these issues, we carefully design and construct a metal-free photocatalytic system through grafting 0D nitrogen-doped graphene quantum dots (N-GQDs) on 2D porous ultrathin carbon nitride (PUCN). The incorporated N-GQDs can act as electron collectors to promote the charge separation/transfer on PUCN, and also can extend the photoabsorption region of PUCN. Thus, the metal-free N-GQDs/PUCN photocatalyst exhibits a drastically enhanced hydrogen production rate of 1248 μmol g^{-1} h^{-1}, which fetches up to about 208 times as high as that of PUCN (6 μmol g^{-1} h^{-1}). Notably, the photocatalytic performance of N-GQDs/PUCN is close to that of Pt/PUCN with the same cocatalyst amount (1706 μmol g^{-1} h^{-1}), and metal-free N-GQDs/PUCN photocatalyst outperforms most of the reported carbon nitride-based photocatalysts with metallic cocatalysts for photocatalytic water splitting. This work offers new insight to construct metal-free carbon nitride-based photocatalysts, which will be beneficial for the practical development of photocatalytic water splitting.

1. Introduction

With economic growth and environmental challenges, it is necessary and urgent to develop sustainable energy for easing energy shortages [1,2]. Solar power, a sustainable and clean energy source, has attracted much attention since the 1970s [3]. Photocatalytic water splitting into hydrogen energy is considered as a most potential strategy for energy conversion [4,5]. After unremitting efforts, researchers have designed and developed a series of semiconductor photocatalysts [6,7]. However, the poor solar-to-hydrogen conversion efficiency of semiconductor photocatalysts seriously restricts the practical development of photocatalytic water splitting, which is due to the poor charge separation/-transfer efficiency, light-harvesting capability and surface reactions [8,9]. Therefore, the development of high performing photocatalysts is necessary to meet this challenge [10,11]. In recent years, carbon nitride ($g\text{-}C_3N_4$) quite gets solicitude for photocatalytic water splitting owing to its excellent physical properties and adjustable composition/morphology/chemical structure [12–14]. Unfortunately, most carbon nitride-based photocatalysts limited by the low light utilization efficiency ($\lambda < 470$ nm), the tardy rate of charge transfer from the inside phase to the surface, and limited active sites [15,16]. Various strategies of crystallinity engineering, defect engineering, morphology control, heterojunction construction and element doping have been developed to achieve efficient photocatalytic water splitting of carbon nitride-based photocatalysts [17,18]. In particular, 2D porous ultrathin carbon nitride (PUCN) possesses stronger redox capacity to increase the catalyst performance than bulk $g\text{-}C_3N_4$ due to the strong quantum effect [19,20]. The unique morphology of PUCN has a larger specific surface, which is beneficial to accelerate surface oxidation-reduction reactions. Although the creation of ultrathin and porous structure can exhibit high hydrogen

* Corresponding authors.
E-mail addresses: zhaomo@ujs.edu.cn (Z. Mo), wangl@shu.edu.cn (L. Wang), xh@ujs.edu.cn (H. Xu).

https://doi.org/10.1016/j.jece.2023.109801
Received 17 February 2023; Received in revised form 14 March 2023; Accepted 25 March 2023
Available online 27 March 2023

evolution rate, the carbon nitride-based photocatalytic water splitting still needs noble metals (for instance Pd, Ag, Pt, and Au) cocatalyst [21]. Noble metals with a large work function can form schottky barrier with g-C_3N_4, which not only can be regarded as an excellent electron capture trap to accelerate the electron transfer process, but also can effectively reduce the energy barrier of hydrogen evolution reaction [22]. However, high price and scarcity of precious metal limit their widespread use, massive efforts has been carried out to develop noble-metal-free cocatalysts for high-performance photocatalytic water splitting [23].

Recently, earth-abundant transition metals (for instance Cu, Ni, Co, and Fe), transition-metal-based cocatalysts and nanocarbon-based substances have been widely used to substitute the noble metals cocatalyst for photocatalytic water splitting [24–26]. Among them, graphene quantum dots (GQDs) are late-stage 0D luminescent nanomaterials in the nanocarbon-based substances with sizes smaller than 10 nm [27]. They are widely used because of their good electronic properties, water solubility, unique properties of non-toxicity and intense photoluminescence, while are attracting more and more attention in the field of photocatalytic water splitting [28]. Doping is an significant method to optimize the energy band structure and optical properties of GQDs [29]. Due to the abundant amino groups as ionic groups, nitrogen-doped GQDs (N-GQDs) possess better visible light absorption, electrical conductivity and abundant edge activity sites than GQDs [29]. Their inherent conjugated π structure not only provides good electron storage and transfer, but also promotes hybridization with other semiconductors. It is expected that the introduction of N-CQDs as noble-metal-free cocatalyst can accelerate charge migration between semiconductors and enhance the separation of space charge carriers. This offered a new possibility for the development of hybrid nanomaterials with high photocatalytic activity. Chen and co-workers employed N-CQDs co-catalysts to realize the efficient charge separation of BiO_{2-x} nanosheets [30]. Recently, N-CQDs co-catalysts were

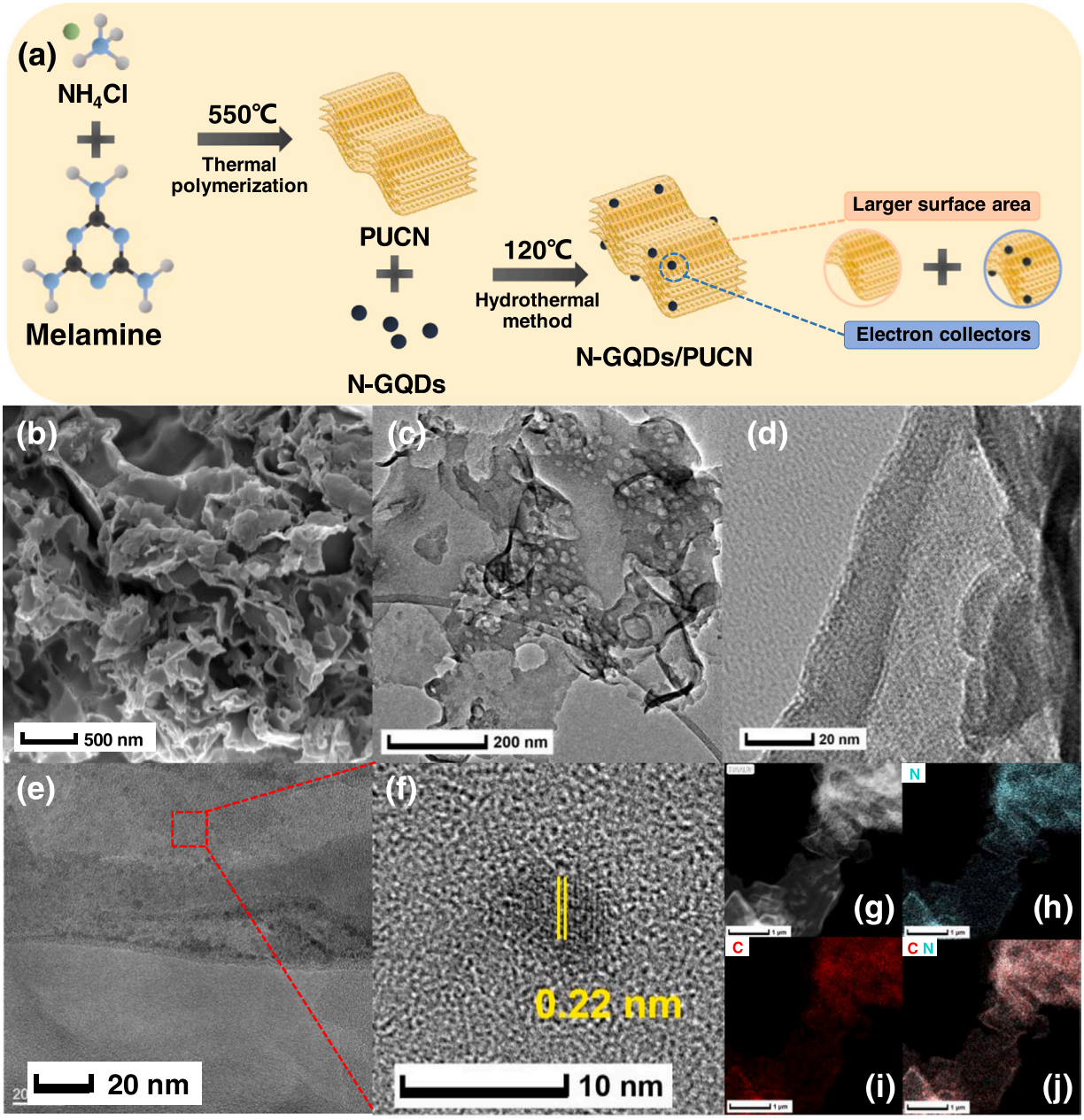

Fig. 1. (a) Schematic illustration for the preparation of N-GQDs/PUCN. (b) SEM image of 2 wt% N-GQDs/PUCN. (c-d) TEM images of 2 wt% N-GQDs/PUCN. (e) HRTEM images of N-GQDs/PUCN. (f-j) EDS elemental mappings of 2 wt% N-GQDs/PUCN.

introduced into a series of semiconductor photocatalysts for achieving excellent hydrogen evolution performance [27]. To this end, direct anchoring 0D N-CQDs onto 2D PUCN should be an alternative approach to form cost-effective photocatalytic system for water splitting.

In this work, metal-free N-GQDs/PUCN photocatalysts based on 0D N-CQDs anchored on 2D PUCN for photocatalytic water splitting is successfully constructed, which considerably enhances the photocatalytic performance of PUCN. Detailed characterization studies show that the N-GQDs/PUCN photocatalyst has several advantages. First of all, the intimate interfacial contact between N-GQDs and PUCN is conducive to the formation of high-quality interfaces, which can accelerate the charge separation/transfer. Secondly, the incorporated N-GQDs can be acted as co-catalyst, which is beneficial to charge separation/transfer and also broaden the light absorption range of PUCN. Among them, the 2 wt% N-GQDs/PUCN has the best photocatalytic activity, the hydrogen generation rate of 1248 μmol g^{-1} h^{-1}, which fetches up to about 208 times as high as that of PUCN. Significantly, the photocatalytic performance of N-GQDs/PUCN is close to that of Pt/PUCN (1706 μmol g^{-1} h^{-1}), which signifies N-GQDs can be used to substitute the noble metals cocatalyst for photocatalytic water splitting.

2. Results and discussion

As illustrated in Fig. 1a, N-GQDs were successfully loaded on the surface of PUCN by a solvothermal method to prepare metal-free N-GQDs/PUCN photocatalyst. Scanning electron microscope (SEM), element mapping, transmission electron microscope (TEM) and high-resolution TEM (HRTEM) were utilized to investigate the morphology and composition of 2 wt% N-GQDs/PUCN (Fig. 1b-j). SEM and TEM images (Fig. 1b,c) show that PUCN possesses a porous ultrathin structure. This is mainly because during the preparation of PUCN, hydrochloric acid (HCl) and ammonia (NH_3) escape and corrode the porous channels on the surface of PUCN, resulting in the formation of porous ultrathin structure. It can be seen from the TEM image (Fig. 1d,e) that N-GQDs are spread over the surface of PUCN, and its average size range is about 5–8 nm. The HRTEM image (Fig. 1f) clearly shows the crystal structure of the N-GQDs with lattice spacing of 0.22 nm, corresponding to the (100) lattice plane of a crystalline graphitic structure [31]. The element mapping images show that the surface of 2 wt% N-GQDs/PUCN photocatalyst is evenly distributed with C and N element (Fig. 1g-j). The crystal and chemical structures of PUCN and N-GQDs/PUCN were analyzed by X-ray diffraction (XRD) characterization. XRD pattern of PUCN (Fig. 2a) obviously shows a strong diffraction peak at 27.3°correspond to the (002) crystal plane of typical graphite interlayer, which belongs to the in-plane stacked diffraction peaks of g-C_3N_4 [32]. The diffraction patterns of N-GQDs/PUCN are similar to that of PUCN, manifesting that the introduction of N-GQDs has minimal impact on the chemical structure of PUCN. Fourier transform infrared spectroscopy (FT-IR) characterization can further verify the chemical structure of N-GQDs/PUCN (Fig. S1). The broad peaks range from 3000 to 3600 cm^{-1} are allocated to the stretching vibrations of the N-H bond of the amine group and the O-H bond of the hydroxyl group and the residual absorbed H_2O [33]. Meanwhile, the peaks from 1200 to 1700 cm^{-1} are belonging to C-N and heterocycles, and the peak at 807 cm^{-1} are the breathing vibration modes of tri-s-triazine unites [34,35]. The above information shows that the basic crystal structure of PUCN is not broken after the introduction of N-GQDs. The successful introduction of N-GQDs can be further verified by the Raman spectrum (Fig. 2b), two typical peaks at 1586 cm^{-1} and 1344 cm^{-1} are observed, which are assigned to the crystalline G band and the disordered D band of N-GQDs, respectively [31,36–38]. The above two weak peaks can also be found in N-GQDs/PUCN, this is probably due to the small doping amount of N-GQDs. X-ray photoelectron spectroscopy (XPS) spectra can dissect the element composition of PUCN and 2 wt% N-GQDs/PUCN (Figs. 2c,d and S2). XPS survey spectra show three signals at 288.0, 399.0 and 532.0 eV, which belong to C 1s, N 1s, and O 1s, respectively (Fig. S2c). The observation of O 1s in the PUCN and 2 wt% N-GQDs/PUCN is largely thanks to the adsorbed water on the surface [39]. The C 1s high-resolution spectra of PUCN (Fig. 2c) shows three peaks are positioned at 284.3, 286.1 and 287.7 eV belong to C-C, C-NH_2 and N-C-N_2,

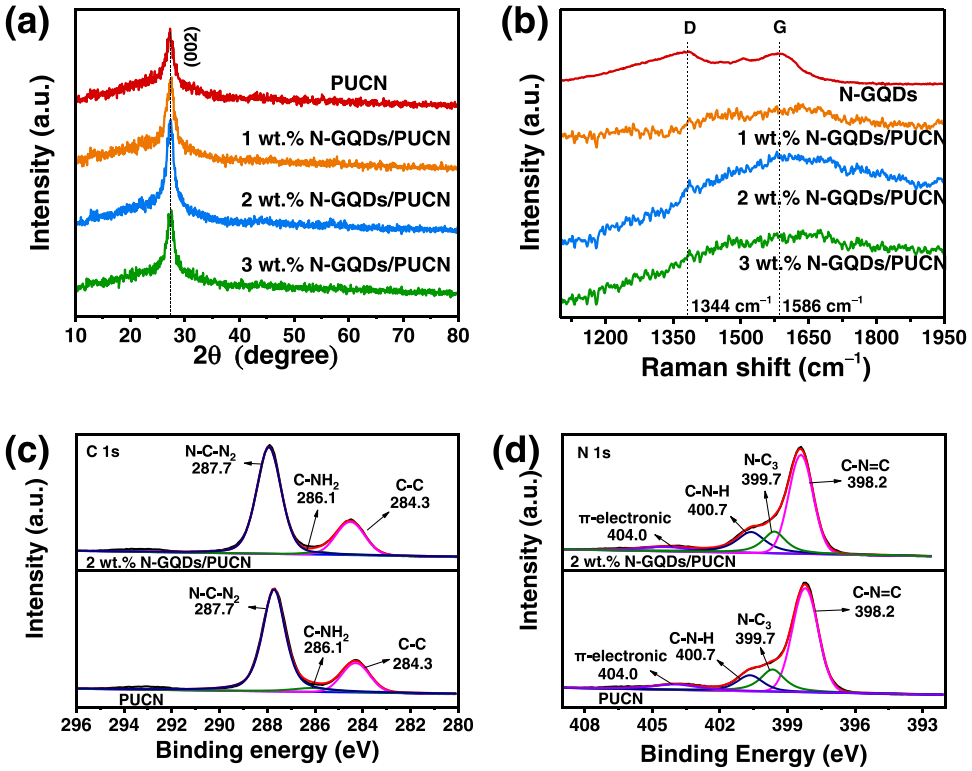

Fig. 2. (a) XRD patterns and (b) Raman spectra of PUCN and N-GQDs/PUCN. XPS spectra of PUCN and 2 wt% N-GQDs/PUCN: (c) C 1s and (d) N 1s.

respectively [40,41]. Similar C species are also resolved by C 1s high-resolution spectra of 2 wt% N-GQDs/PUCN, indicating the incorporated N-GQDs do not change the coordination environment of PUCN. In Fig. 2d, the high-resolution N 1s spectra of 2 wt% N-GQDs/PUCN match well with that of PUCN due to the low ratio of N-GQDs. Specifically, the high-resolution N 1s spectra shows four peaks at about 398.2 (N1), 399.7 (N2), 400.7 (N3), and 404.0 eV (N4), corresponding to sp^2-hybridized N in the triazine ring (C═N-C), tertiary N group (N-C_3), amino group (C-N-H), and π electronic excitation, respectively [42] . The results of HRTEM, XRD, FT-IR, Raman spectrum and XPS spectra together confirm that the N-GQDs really exist in the N-GQDs/PUCN photocatalyst, and the incorporated N-GQDs cause no structural damage of PUCN.

As presented in Fig. 3a, the hydrogen evolution performance of PUCN and N-GQDs/PUCN were measured under visible light ($\lambda \geq 400$ nm) irradiation. PUCN has a low photocatalytic hydrogen production rate of 6 μmol g^{-1} h^{-1}. With the introduction of N-GQDs, the composite materials significantly increased the catalytic performance. The hydrogen evolution of 1 wt%, 2 wt%, and 3 wt% N-GQDs/PUCN reached as 411, 1248, and 529 μmol g^{-1} h^{-1}. The optimal loading ratio of 2 wt% N-GQDs/PUCN was about 208 times comparable to PUCN. It proved that the incorporation of N-GQDs can act as noble-metal-free cocatalysts to promote the photocatalytic hydrogen evolution reaction obviously. However, when further increasing N-GQDs/PUCN ratio to 3 wt%, the photocatalytic activity of N-GQDs/PUCN is lowered to some extent. That may be due to the excess N-GQDs would lead to the light shielding effect in N-GQDs/PUCN composite, resulting in a certain deactivation of light adsorption capability [43]. Meanwhile, the photocatalytic stability of 2 wt% N-GQDs/PUCN is investigated by cycling experiment under visible light irradiation. As shown in Fig. 3b, after 5 cycles, the activity of the 2 wt% N-GQDs/PUCN only shows slight declines due to the consumption of triethanolamine (TEOA) [44], and the XRD, FT-IR and HRTEM data (Figs. 3c, S3 and S4) of 2 wt% N-GQDs/PUCN has not changed obviously, indicating that N-GQDs/PUCN has good stability [45,46]. The apparent quantum efficiency (AQE) trend line shows an agreement with the UV–visible absorption spectra, its corresponding value of 2 wt% N-GQDs/PUCN with central wavelengths of 405 and 420 nm are 11.5% and 0.9% (Fig. 3d and table S1). Therefore, the above results demonstrate that the metal-free N-GQDs/PUCN is a promising and efficient photocatalyst.

The optical properties of PUCN and N-GQDs/PUCN were explored in depth by UV–visible absorption spectra (Fig. 4a). The PUCN presents a clear absorption edge at ca. 460 nm, and the introduction of N-GQDs leads to a significant growth of the light absorption within the visible range, which results in an enhanced utilization of visible light [47]. This can help to generate a large number of carriers to participate in the photocatalytic reduction reaction [48]. To further explore the carrier separation/transfer behavior of N-GQDs/PUCN, steady-state photoluminescence (PL), photocurrent, and electrochemical impedance (EIS) tests were carried out. The PL spectra (Fig. 4b) were obtained by excited at 460 nm and the strong emission peaks was observed in PUCN and N-GQDs/PUCN. Compared with PUCN, the fluorescence intensity of 2 wt% N-GQDs/PUCN was significantly decreased, which suggests that the introduction of N-GQDs increased the carrier separation efficiency [49]. This is because the incorporated N-GQDs can efficiently extract electrons from PUCN to promote the charge separation/transfer. Correspondingly, the photocurrent test results in Fig. 4c. Compared with PUCN, the photocurrent intensity of 1 wt%, 2 wt%, and 3 wt% N-GQDs/PUCN in 0.1 M phosphate buffer (pH = 7.0) are improved to a certain extent, which indicates a faster carrier separation/transfer performance [50,51]. It is proved that N-GQDs plays an important role in electron transport paths. The results of EIS were measured in 0.1 M phosphate buffer and 5 mM $K_3[Fe(CN)_6]/K_4[Fe(CN)_6]$ (pH = 7.0), which were presented in EIS Nyquist plots (Fig. 4d). Compared with PUCN, the charge transfer resistance of 1 wt%, 2 wt%, and 3 wt% N-GQDs/PUCN are lower, which suggests the beneficial charge transportation in N-GQDs/PUCN by the intimate interfacial contact between N-GQDs and PUCN [52–54]. It is consistent with the result that the implantation of N-GQDs can reduce the charge transfer barrier and increase the charge density of PUCN.

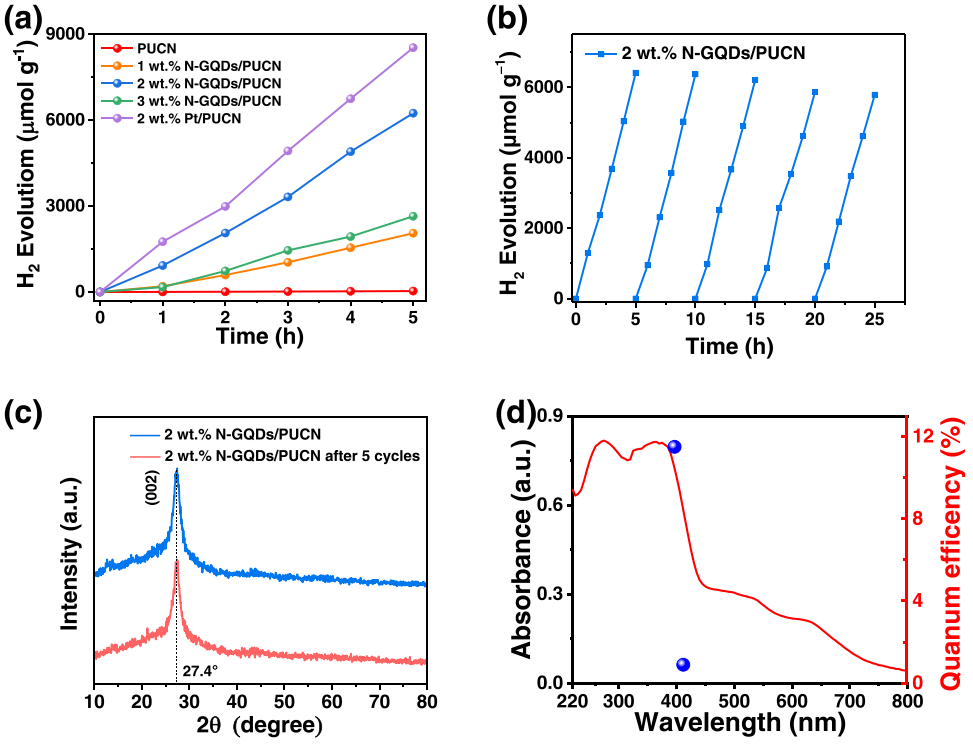

Fig. 3. (a) Photocatalytic hydrogen evolution over PUCN and N-GQDs/PUCN. (b) Photocatalytic stability of 2 wt% N-GQDs/PUCN. (c) XRD spectra of 2 wt% N-GQDs/PUCN before and after photocatalytic reaction. (d) AQE of 2 wt% N-GQDs/PUCN with different monochromatic wavelengths.

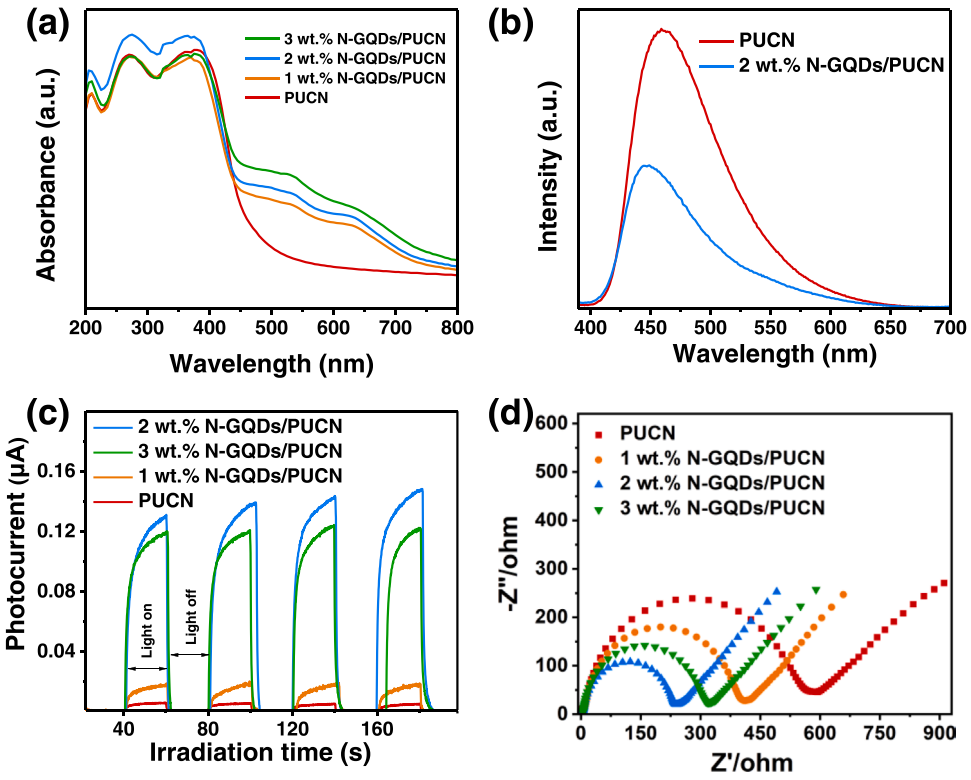

Fig. 4. (a) UV–vis DRS, (b) Room-temperature PL spectra, (c) Transient photocurrent representation in 0.1 M phosphate buffer (pH = 7.0) and (d) EIS Nyquist plots of PUCN and N-GQDs/PUCN in 0.1 M phosphate buffer and 5 mM $K_3[Fe(CN)_6]/K_4[Fe(CN)_6]$ (pH = 7.0).

To understand the band structure of GQDs/PUCN, the bandgaps values of PUCN is estimated to be 2.87 eV according to Kubelka-Munk function in Fig. 5a. The valence band (VB) are recorded to determine the position of PUCN, which is about 1.67 V (Fig. 5b). Therefore, the VB potential of PUCN is more negative than the reduction potential of H^+/H_2 (0 V *vs.* NHE), which thermodynamically favors hydrogen evolution reaction. As displayed in Fig. 5c, the flat-band potential of PUCN is measured by the Mott-Schottky plots, which is determined to be − 1.20 V [55]. The conduction band (CB) potential of PUCN can be nearly equal to the flat-band potential of PUCN because g-C_3N_4 is a n-type semiconductor, so the CB potential of PUCN is − 1.20 V (*vs.* NHE).[49] The photocatalytic mechanism of metal-free N-GQDs/PUCN photocatalyst was proposed in Fig. 6. Under simulated sunlight, the electrons in the VB of PUCN are excited and transferred to CB of PUCN, along with the remaining holes in the VB of PUCN. Then, the incorporated N-GQDs can be acted as electron collectors to extract electrons from PUCN, thus facilitating the transfer of photogenerated electrons across the dense interface from PUCN to N-GQDs. Finally, N-GQDs play the role of guiding electrons to participate in the hydrogen generation reaction.

3. Conclusions

In summary, we develop a metal-free N-GQDs/PUCN photocatalyst composed of low-content dispersed 0D N-GQDs onto 2D PUCN. The as-prepared N-GQDs/PUCN displays good photocatalytic hydrogen evolution activity (1248 μmol g^{-1} h^{-1}), which is every bit a peer to the same amount of Pt/PUCN. The greatly raised photocatalytic performance of N-GQDs/PUCN profits from the enhanced light efficiency and the accelerated charge separation/transfer by the incorporated metal-free cocatalyst N-GQDs. The present metal-free system shows the great potential on the optimization of photocatalytic hydrogen evolution activity via implanting metal-free cocatalyst onto the surface of g-C_3N_4, providing new ideas for the rational design of metal-free carbon nitride-based photocatalysts.

CRediT authorship contribution statement

Hanxiang Chen: Formal analysis, Writing – original draft. **Zhao Mo:** Writing – review & editing, Supervision. **Zeming Wang:** Formal analysis. **Pengcheng Yan:** Data curation. **Peipei Sun:** Software. **Guyu Wu:**

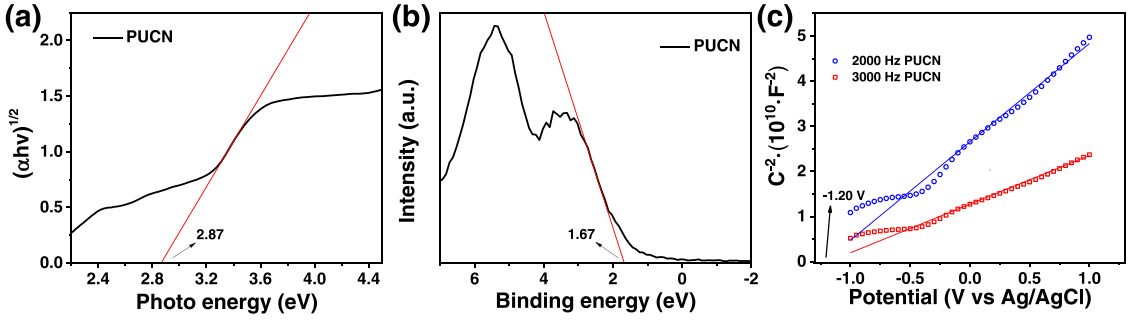

Fig. 5. (a) The estimated bandgaps, (b) VB XPS spectra and (c) Mott-Schottky plots (2000 Hz and 3000 Hz) of PUCN.

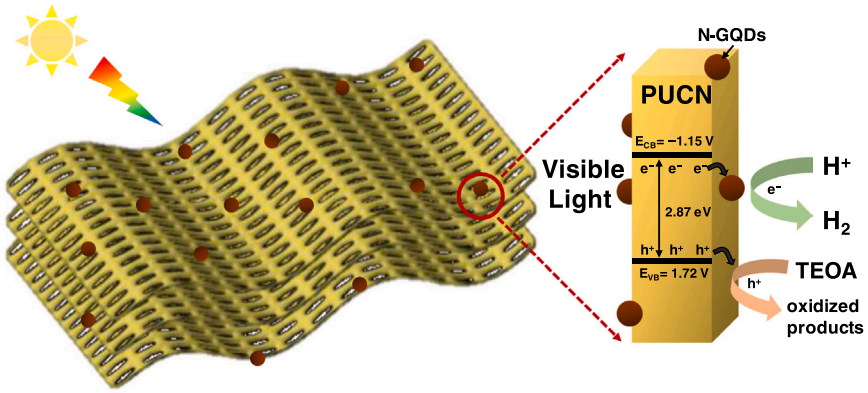

Fig. 6. Schematic illustration of the proposed mechanism for photocatalytic water splitting on metal-free N-GQDs/PUCN.

Formal analysis. **Jinyuan Zhang:** Data curation. **Xianglin Zhu:** Formal analysis. **Liang Wang:** Supervision. **Hui Xu:** Formal analysis, Supervision.

Declaration of Competing Interest

The authors declare that they have no known competing financial interests or personal relationships that could have appeared to influence the work reported in this paper.

Data availability

No data was used for the research described in the article.

Acknowledgments

This study was financially supported by the National Natural Science Foundation of China (22208129, 22202086, 22005123), China Post-doctoral Science Foundation (2021M691305), Jiangsu Province Post-doctoral Science Foundation (2021K079A).

Appendix A. Supplementary material

Supplementary data associated with this article can be found in the online version at doi:10.1016/j.jece.2023.109801.

References

[1] E. Nikoloudakis, I. Lopez-Duarte, G. Charalambidis, K. Ladomenou, M. Ince, A. G. Coutsolelos, Porphyrins and phthalocyanines as biomimetic tools for photocatalytic H_2 production and CO_2 reduction, Chem. Soc. Rev. 51 (2022) 6965–7045.

[2] S. Wang, J. Zhang, B. Li, H. Sun, S. Wang, X. Duan, Morphology-dependent photocatalysis of graphitic carbon nitride for sustainable remediation of aqueous pollutants: a mini review, J. Environ. Chem. Eng. 10 (2022), 107438.

[3] X. Meng, S. Wang, C. Zhang, C. Dong, R. Li, B. Li, Q. Wang, Y. Ding, Boosting hydrogen evolution performance of a CdS-based photocatalyst: in situ transition from type I to type II heterojunction during photocatalysis, ACS Catal. 12 (2022) 10115–10126.

[4] Z. Mo, G. Wu, P. Yan, X. Zhu, J. Qian, Y. Lei, L. Xu, H. Xu, H. Li, Engineering oxygen into ultrathin graphitic carbon nitride: synergistic improvement of electron reduction and charge carrier dynamics for efficient photocatalysis, Mater. Today Chem. 25 (2022), 100956.

[5] J.A.S. Syed, X.-Y. Zhang, W.-J. Ding, A.-D. Li, An overview of the current progress of graphitic carbon nitride and its multifunctional applications, J. Environ. Chem. Eng. 10 (2022), 108745.

[6] L. Dai, A. Dong, X. Meng, H. Liu, Y. Li, P. Li, B. Wang, Enhancement of visible-light-driven hydrogen evolution activity of 2D π-conjugated bipyridine-based covalent organic frameworks via post-protonation, Angew. Chem. Int. Ed. (2023), 202300224.

[7] X. Zheng, Y. Liu, Y. Yang, Y. Song, P. Deng, J. Li, W. Liu, Y. Shen, X. Tian, Recent advances in cadmium sulfide-based photocatalysts for photocatalytic hydrogen evolution, Renewables 1 (2023) 39–56.

[8] Y. Tang, W. Zhou, Q. Shang, Y. Guo, H. Hu, Z. Li, Y. Zhang, L. Liu, H. Wang, X. Tan, T. Yu, J. Ye, Discerning the mechanism of expedited interfacial electron transformation boosting photocatalytic hydrogen evolution by metallic 1T-WS_2-induced photothermal effect, Appl. Catal. B 310 (2022), 121295.

[9] S. Wang, J. Zhang, B. Li, H. Sun, S. Wang, Engineered graphitic carbon nitride-based photocatalysts for visible-light-driven water splitting: a review, Energy Fuels 35 (2021) 6504–6526.

[10] M. Torras, P. Molet, L. Soler, J. Llorca, A. Roig, A. Mihi, Au/TiO_2 2D-photonic crystals as UV-visible photocatalysts for H_2 production, Adv. Energy Mater. 12 (2021), 2103733.

[11] X. Zhu, J. Yang, X. Zhu, J. Yuan, M. Zhou, X. She, Q. Yu, Y. Song, Y. She, Y. Hua, H. Li, H. Xu, Exploring deep effects of atomic vacancies on activating CO_2 photoreduction via rationally designing indium oxide photocatalysts, Chem. Eng. J. 422 (2021), 129888.

[12] J. Yang, L. Jing, X. Zhu, W. Zhang, J. Deng, Y. She, K. Nie, Y. Wei, H. Li, H. Xu, Modulating electronic structure of lattice O-modified orange polymeric carbon nitrogen to promote photocatalytic CO_2 conversion, Appl. Catal. B 320 (2023), 122005.

[13] N. Ishak, V. Jeyalakshmi, M. Setka, M. Grandcolas, B. Devadas, M. Šoóš, Upgrading of g-C_3N_4 semiconductor by a Nitrogen-doped carbon material: a photocatalytic degradation application, J. Environ. Chem. Eng. 11 (2023), 109381.

[14] G. Liu, H. Lv, Y. Zeng, M. Yuan, Q. Meng, Y. Wang, C. Wang, Single-atom Pd-N_3 sites on carbon-deficient g-C_3N_4 for photocatalytic H_2 evolution, Trans. Tianjin Univ. 27 (2021) 139–146.

[15] M. Song, X. Deng, G. Li, Q. Wang, H. Peng, P. Chen, S.-F. Yin, Edge- and bridge-engineering-mediated exciton dissociation and charge separation in carbon nitride to boost photocatalytic H_2 evolution integrated with selective amine oxidation, J. Mater. Chem. A 10 (2022) 16448–16456.

[16] M.R. Ebrahimian, M. Tavakolian, M. Hosseini-Sarvari, From expired metformin drug to nanoporous N-doped-g-C_3N_4: durable sunlight-responsive photocatalyst for oxidation of furfural to maleic acid, J. Environ. Chem. Eng. 11 (2023), 109347.

[17] B. Zhai, H. Li, G. Gao, Y. Wang, P. Niu, S. Wang, L. Li, A crystalline carbon nitride based near-infrared active photocatalyst, Adv. Funct. Mater. (2022), 2207375.

[18] Y. Shao, X. Hao, S. Lu, Z. Jin, Molten salt-assisted synthesis of nitrogen-vacancy crystalline graphitic carbon nitride with tunable band structures for efficient photocatalytic overall water splitting, Chem. Eng. J. 454 (2023), 140123.

[19] B. Wu, L. Zhang, B. Jiang, Q. Li, C. Tian, Y. Xie, W. Li, H. Fu, Ultrathin porous carbon nitride bundles with an adjustable energy band structure toward simultaneous solar photocatalytic water splitting and selective phenylcarbinol oxidation, Angew. Chem. Int. Ed. 60 (2021) 4815–4822.

[20] P. Sha, Y. You, D. Wen, Z. Wu, Q. Wang, D. Bu, S. Huang, Two-dimensional ultrathin graphic carbon nitrides with extended π-conjugation as extraordinary efficient hydrogen evolution photocatalyst, Small 19 (2023), 2205834.

[21] Y. Zhang, J. Zhao, H. Wang, B. Xiao, W. Zhang, X. Zhao, T. Lv, M. Thangamuthu, J. Zhang, Y. Guo, J. Ma, L. Lin, J. Tang, R. Huang, Q. Liu, Single-atom Cu anchored catalysts for photocatalytic renewable H_2 production with a quantum efficiency of 56%, Nat. Commun. 13 (2022) 58.

[22] X. Zhou, Y. Tian, J. Luo, B. Jin, Z. Wu, X. Ning, L. Zhan, X. Fan, T. Zhou, S. Zhang, X. Zhou, MoC quantum dots@N-doped-carbon for low-cost and efficient hydrogen evolution reaction: from electrocatalysis to photocatalysis, Adv. Funct. Mater. 32 (2022), 2201518.

[23] W. Wang, Y. Tao, J. Fan, Z. Yan, H. Shang, D.L. Phillips, M. Chen, G. Li, Fullerene-graphene acceptor drives ultrafast carrier dynamics for sustainable cds photocatalytic hydrogen evolution, Adv. Funct. Mater. 32 (2022), 2201357.

[24] H. Zhao, L. Jian, M. Gong, M. Jing, H. Li, Q. Mao, T. Lu, Y. Guo, R. Ji, W. Chi, Y. Dong, Y. Zhu, Transition-metal-based cocatalysts for photocatalytic water splitting, Small Struct. 3 (2022), 2100229.

[25] L. Ai, R. Shi, J. Yang, K. Zhang, T. Zhang, S. Lu, Efficient combination of G-C_3N_4 and CDs for enhanced photocatalytic performance: a review of synthesis, strategies, and applications, Small 17 (2021), 2007523.

[26] H. Yu, R. Shi, Y. Zhao, G.I. Waterhouse, L.Z. Wu, C.H. Tung, T. Zhang, Smart utilization of carbon dots in semiconductor photocatalysis, Adv. Mater. 28 (2016) 9454–9477.

[27] A. Ghaffarkhah, E. Hosseini, M. Kamkar, A.A. Sehat, S. Dordanihaghighi, A. Allahbakhsh, C. van der Kuur, M. Arjmand, Synthesis, applications, and

prospects of graphene quantum dots: a comprehensive review, Small 18 (2022), 2102683.
[28] B.J. Moon, S.J. Kim, A. Lee, Y. Oh, S.K. Lee, S.H. Lee, T.W. Kim, B.H. Hong, S. Bae, Structure-controllable growth of nitrogenated graphene quantum dots via solvent catalysis for selective C-N bond activation, Nat. Commun. 12 (2021) 5879.
[29] P. Kumar, C. Dhand, N. Dwivedi, S. Singh, R. Khan, S. Verma, A. Singh, M.K. Gupta, S. Kumar, R. Kumar, A.K. Srivastava, Graphene quantum dots: a contemporary perspective on scope, opportunities, and sustainability, Renew. Sustain. Energy Rev. 157 (2022), 111993.
[30] F. Chen, L.-L. Liu, Y.-J. Zhang, J.-H. Wu, G.-X. Huang, Q. Yang, J.-J. Chen, H.-Q. Yu, Enhanced full solar spectrum photocatalysis by nitrogen-doped graphene quantum dots decorated BiO_{2-x} nanosheets: ultrafast charge transfer and molecular oxygen activation, Appl. Catal. B 277 (2020), 119218.
[31] L. Wang, W. Li, B. Wu, Z. Li, D. Pan, M. Wu, Room-temperature synthesis of graphene quantum dots via electron-beam irradiation and their application in cell imaging, Chem. Eng. J. 309 (2017) 374–380.
[32] G. Wu, Z. Mo, P. Sun, Z. Cao, X. Zhu, Y. Song, Y. Wei, X. She, H. Li, H. Xu, Improved atomic hydrogen desorption by Cu_3N with suitable electronic structure to enhance photocatalytic H_2 evolution, Mater. Today Energy 29 (2022), 101111.
[33] P. Yan, Y. Jin, L. Xu, Z. Mo, J. Qian, F. Chen, J. Yuan, H. Xu, H. Li, Enhanced photoelectrochemical aptasensing triggered by nitrogen deficiency and cyano group simultaneously engineered 2D carbon nitride for sensitively monitoring atrazine, Biosens. Bioelectron. 206 (2022), 114144.
[34] Z. Yu, X. Yue, J. Fan, Q. Xiang, Crystalline intramolecular ternary carbon nitride homojunction for photocatalytic hydrogen evolution, ACS Catal. 12 (2022) 6345–6358.
[35] K. Lu, Q. Wei, X. Bao, Z. Xiao, X. Cheng, X. Liu, Z. Wang, H. Li, B. Huang, Photocharged carbon nitride with local electron accumulation: towards outstanding round-the-clock hydrogen peroxide production, Appl. Surf. Sci. 609 (2023), 155242.
[36] Q. Hao, Z. Li, Y. Shi, R. Li, Y. Li, S. Ouyang, H. Yuan, T. Zhang, Boron-doped CN supported metallic Co catalysts with interfacial electron transfer for enhanced photothermal CO hydrogenation, Nano Energy 102 (2022), 107723.
[37] R. Shi, Z. Li, H. Yu, L. Shang, C. Zhou, G.I.N. Waterhouse, L.Z. Wu, T. Zhang, Effect of nitrogen doping level on the performance of N-doped carbon quantum Dot/TiO_2 composites for photocatalytic hydrogen evolution, ChemSusChem 10 (2017) 4650–4656.
[38] S. Wu, D. Deng, E. Zhang, H. Li, L. Xu, CoN nanoparticles anchored on ultra-thin N-doped graphene as the oxygen reduction electrocatalyst for highly stable zinc-air batteries, Carbon 196 (2022) 347–353.
[39] Z. Li, Y. Chen, X. Chen, L. Li, S. Kuang, Y. Guo, Y. Wang, J. Gao, Artificial visible light-induced H_2O_2 production using polymeric K/O-doped carbon nitride as a catalyst, Appl. Surf. Sci. 609 (2023), 155432.
[40] Z. Gong, L. Chen, K. Chen, S. Gou, X. Zhao, L. Song, J. Ma, L. Han, Significantly improved photocatalytic H_2O_2 generation over PDA-modified g-C_3N_4 via promoting charge-carriers separation and oxygen adsorption, J. Environ. Chem. Eng. 11 (2023), 109405.
[41] L. Xu, S. Wu, X. He, H. Wang, D. Deng, J. Wu, H. Li, Interface engineering of anti-perovskite Ni_3FeN/VN heterostructure for high-performance rechargeable zinc-air batteries, Chem. Eng. J. 437 (2022), 135291.
[42] L. Xu, W. Duan, F. Chen, J. Zhang, H. Li, A photoelectrochemical aptasensor for the determination of bisphenol A based on the Cu (I) modified graphitic carbon nitride, J. Hazard. Mater. 400 (2020), 123162.
[43] F. Lin, S. Zhou, G. Wang, J. Wang, T. Gao, Y. Su, C.-P. Wong, Electrostatic self-assembly combined with microwave hydrothermal strategy: construction of 1D/1D carbon nanofibers/crystalline g-C_3N_4 heterojunction for boosting photocatalytic hydrogen production, Nano Energy 99 (2022), 107432.
[44] Z. Mo, H. Xu, Z. Chen, X. She, Y. Song, J. Lian, X. Zhu, P. Yan, Y. Lei, S. Yuan, H. Li, Construction of MnO_2/monolayer g-C_3N_4 with Mn vacancies for Z-scheme overall water splitting, Appl. Catal. B 241 (2019) 452–460.
[45] P. Yan, F. Ji, W. Zhang, Z. Mo, J. Qian, L. Zhu, L. Xu, Engineering surface bromination in carbon nitride for efficient CO_2 photoconversion to CH_4, J. Colloid Interface Sci. 634 (2023) 1005–1013.
[46] X.-X. Xing, H.-L. Guo, T.-M. He, X. An, H.-P. Li, W.-S. Zhu, H.-M. Li, J.-Y. Pang, D.-B. Dang, Y. Bai, Tungstovanadate-based ionic liquid catalyst $[C_2(MIM)_2]_2VW_{12}O_{40}$ used in deep desulfurization for ultraclean fuel with simultaneous recovery of the sulfone product, ACS Sustain. Chem. Eng. 10 (2022) 11533–11543.
[47] Y. Chen, M. Yang, Y. Jia, P. Yan, F. Chen, J. Qian, L. Xu, H. Li, NiS_2/NiFe LDH/g-C_3N_4 ternary heterostructure-based label-free photoelectrochemical aptasensing for highly sensitive determination of enrofloxacin, Mater. Today Chem. 24 (2022), 100845.
[48] J. Di, C. Chen, Y. Wu, Y. Zhao, C. Zhu, Y. Zhang, C. Wang, H. Chen, J. Xiong, M. Xu, J. Xia, J. Zhou, Y. Weng, L. Song, S. Li, W. Jiang, Z. Liu, Polarized Cu-Bi site pairs for non-covalent to covalent interaction tuning toward N_2 photoreduction, Adv. Mater. 34 (2022), 2204959.
[49] P. Sun, Z. Mo, H. Chen, Y. Song, J. Liu, W. Yin, H. Dai, Z. Chen, H. Li, H. Xu, Highly efficient photosynthesis of H_2O_2 via two-channel pathway photocatalytic water splitting, Inorg. Chem. Front. 9 (2022) 1701–1707.
[50] C. Zhu, Q. He, W. Wang, F. Du, F. Yang, C. Chen, C. Wang, S. Wang, X. Duan, S-scheme photocatalysis induced by $ZnIn_2S_4$ nanoribbons-anchored hierarchical CeO_2 hollow spheres for boosted hydrogen evolution, J. Colloid Interface Sci. 620 (2022) 253–262.
[51] J. Di, C. Chen, C. Zhu, R. Long, H. Chen, X. Cao, J. Xiong, Y. Weng, L. Song, S. Li, H. Li, Y. Xiong, Z. Liu, Surface local polarization induced by bismuth-oxygen vacancy pairs tuning non-covalent interaction for CO_2 photoreduction, Adv. Energy Mater. 11 (2021), 2102389.
[52] J. Dong, F. Chen, L. Xu, P. Yan, J. Qian, Y. Chen, M. Yang, H. Li, Fabrication of sensitive photoelectrochemical aptasensor using Ag nanoparticles sensitized bismuth oxyiodide for determination of chloramphenicol, Microchem. J. 178 (2022), 107317.
[53] Y. Zhang, J. Di, X. Zhu, M. Ji, C. Chen, Y. Liu, L. Li, T. Wei, H. Li, J. Xia, Chemical bonding interface in $Bi_2Sn_2O_7$/BiOBr S-scheme heterojunction triggering efficient N_2 photofixation, Appl. Catal. B 323 (2023), 122148.
[54] Y.H. Fan, M. Du, Y.X. Li, W.J. Zhu, J.Y. Pang, Y. Bai, D.B. Dang, Construction of water-stable rare-earth organic frameworks with ambient high proton conductivity based on zirconium sandwiched heteropolytungstate, Inorg. Chem. 61 (2022) 13829–13835.
[55] C. Zhu, H. Yao, S. Le, Y. Yin, C. Chen, H. Xu, S. Wang, X. Duan, S-scheme photocatalysis induced by ultrathin TiO_2(B) nanosheets-anchored hierarchical In_2S_3 spheres for boosted photocatalytic activity, Compos. Part B Eng. 242 (2022), 110082.